Cellular and Molecular Neurobiology (2019) 39:301–319
https://doi.org/10.1007/s10571-019-00654-y

ORIGINAL RESEARCH

Myosin IIA Regulated Tight Junction in Oxygen Glucose-Deprived Brain Endothelial Cells Via Activation of TLR4/PI3K/Akt/JNK1/2/14-3-3ε/NF-κB/MMP9 Signal Transduction Pathway

Yanni Lv[1] · Wen Liu[2] · Zhaohui Ruan[1] · Zixuan Xu[1] · Longsheng Fu[1]

Received: 25 October 2018 / Accepted: 14 January 2019 / Published online: 21 January 2019

Abstract
Non-muscle myosin heavy chain IIA (NMMHC IIA), a member of Myosin II family, plays a critical role in various cellular physiological processes. Our previous research had suggested that NMMHC IIA could participate in regulating tight junction morphological changes induced by ischemia stroke. Thus, in the current study, we attempted to uncover the regulation pattern of NMMHC IIA on tight junction dysfunction in oxygen glucose-deprived (OGD) mouse brain bEND.3 endothelial cells. The regulation of NMMHC IIA on tight junction in OGD-stimulated bEND.3 cells was evaluated by western blotting assay. Morphologic change of occludin, claudin-5, and ZO-1 tight junction proteins was compared with pretreatment with NMMHC II inhibitor blebbistatin via immunohistochemical staining. Detection of activation of NMMHC IIA on OGD-mediated tight junction transduction pathway was investigated via Koch's postulate using corresponding protein inhibitor. Our results showed that NMMHC IIA was activated in OGD-stimulated bEND.3 endothelial cells. The inhibition of NMMHC IIA could attenuate the morphologic change of occludin, claudin-5, and ZO-1 tight junction proteins. NMMHC IIA participated in regulating downstream transduction pathway TLR4, phosphatidylinositol 3-kinase (PI3K), Akt, JNK1/2, 14-3-3ε, nuclear factor kappa B (NF-κB) and matrix metalloprotein 9 (MMP9). Blocking of these pathways using indicated inhibitors demonstrated that NMMHC IIA destroyed the connection of tight junction via the activation of TLR4/PI3K/Akt/JNK1/2/14-3-3ε/NF-κB/MMP9 pathway. Our study described the key role of NMMHC IIA in OGD-stimulated mouse brain bEND.3 endothelial cells, while also exhibited the molecule effect on tight junction dysfunction via TLR4/PI3K/Akt/JNK1/2/14-3-3ε/NF-κB/MMP9 signal transduction pathway.

Keywords Non-muscle myosin heavy chain IIA · Mouse brain bEND.3 endothelial cells · Tight junction dysfunction · TLR4/PI3K/Akt/JNK1/2/14-3-3ε/NF-κ/BMMP9

Introduction

BBB compromise is a hallmark of stroke, when the BBB suffers a damage, such as ischemia or trauma, resulting in the structural changes constructed of the tight junction (TJ) proteins between adjacent endothelial cells (Luissint et al. 2012; Greene et al. 2016). TJ dysfunction gave rise to cascading inflammatory responses and succedent morphological changes of tight junction (Stamatovic et al. 2016). The driving power behind these dramatic changes is produced by reorganization of myosin cytoskeletal structure, which is consisted of non-muscle myosin II and actin (Wickman et al. 2013). Myosin II is a molecular motor that hydrolyzed through ATP to convert chemical energy into mechanical force that bound and contracted actin (Butt et al. 2010). Myosin II exists in non-muscle cells, called non-muscle myosin heavy chains (NMMHCs). In addition to providing power for intracellular molecular movement, NMMHCs also was involved in various cellular physiological activities, such as cell migration, adhesion, cytokinesis, vesicle metastasis, endocytosis, and gene transcription. The NMMHCs are encoded by three genes, MYH9, MYH10, and MYH14, that named three isoforms, i.e., NMMHC IIA, MMMHC IIB, and MMMHC IIC (Clark et al. 2008).

✉ Yanni Lv
lvyanni@126.com

[1] Pharmacy department, The First Affiliated Hospital of Nanchang University, Nanchang 330006, Jiangxi, China

[2] Jiangxi Provincial Institute of Traditional Chinese Medicine, Nanchang 330006, Jiangxi, China

Mashukova A revealed that TJ dysfunction was obvious in aPKC knockdown confluent Caco-2 monolayers, upregulating the expression of NMMHC IIA (MYH9) could attenuate the TJ damage, while the change of NMMHC IIB (MYH10) and NMMHC IIC (MYH14) levels did not have an impact on the TJ (Mashukova et al. 2011), also previous studies have suggested the same results (Utech et al. 2005). In addition, NMMHC IIA highlights its unique role in the adjustment and control of epithelial adherens by exerting functions on tight junctions in mammalian epithelia (Ivanov et al. 2007). Although the relationship of NMMHC IIA and TJ has been reported, the exact mechanism of NMMHC IIA still remains unexplored.

Previous work had revealed that NMMHC IIA, TLR4-mediated PI3K/AKT/JNK1/2/14-3-3ε signaling pathway explored the mechanism underlying Blood–Brain–**B**arrier dysfunction via the tight junction pathway (Lv et al. 2018). Two hours of ischemia stroke not only activated the expression of NMMHC IIA, but also activated the expression of TLR4, p-PI3K, PI3K, p-AKT, AKT, p-JNK1/2, p-JNK1/2, p-Bad (S136), Bad (S136), p-Bad (S128), Bad (S128), 14-3-3ε, NF-κB p-p65, and NF-κB p65. However, the compelling evidence involved in NMMHC IIA modulating TJ in endothelial cells was not clear. In the present study, we sought to determine the possible regulation effect of NMMHC IIA on tight junction in oxygen glucose-deprived (OGD) brain endothelial cells via TLR4/PI3K/Akt/JNK1/2/14-3-3ε/NF-κB/MMP9 signal transduction pathway. The effect of NMMHC IIA on the expression of occludin, claudin-5, ZO-1, TLR4, phosphatidylinositol 3-kinase (PI3K), Akt, JNK1/2, 14-3-3ε, nuclear factor kappa B (NF-κB) pathway, and MMP9 were evaluated by immunohistochemical staining and western blotting assay. Meanwhile, the reliable chain of transduction signaling pathway and the underlying mechanism were investigated via Koch's postulate using corresponding protein inhibitor. We hoped that our findings on NMMHC IIA could facilitate to underlie the mechanism of the progression of ischemia stroke. In vivo and in vitro findings would exhibit a key role of NMMHC IIA in TJ expression and ischemia stroke pathological process.

Materials and Methods

Animals and Cells Culture

C57BL/6J mice weighing 18–22 g were purchased from the Yangzhou University Model Animal Research Center (Certificate No. SCXK 2017-0004) and raised in a 12-h light–dark cycle in the laboratory of The First Affiliated Hospital of Nanchang University. All animal care-related procedures were based on the National Institutes of Health Guide for the use of Laboratory Animals. All the experimental items were approved by Institutional Animal Care and use Committee of Nanchang University. All efforts were aimed at minimizing the pain of animals and the number of animals used. Before performing the experiments, all animals were randomized into experimental groups, and the indices were measured by operators blinded to the study procedures. Mouse brain bEND.3 endothelial cells were purchased from the Bioleaf Biotech (Shanghai, China). Cell were cultured in RPMI 1640 (Invitrogen, USA) and supplemented with 15% fetal bovine serum (FBS, Sigma, USA), 100 U/mL penicillin, and 100 U/mL streptomycin (Ameresco, USA) at 37 °C in a humidified atmosphere of 5% CO2 and 95% air. The density difference of the bEND.3 endothelial cells on the plate was carefully minimized. blebbistatin and all other chemicals used were obtained from Sigma Chemicals (Sigma-Aldrich, USA, B0560).

Co-immunoprecipitation

According to the instructions of Pierce™ Direct IP Kit (Thermo Fisher Scientific, 26148, CN) 20 µl Amino Link Plus Resin and Pierce control Agarose Resin (negative control) were applied to incubate with 4 µg NMMHC **IIA** rabbit monoclonal for 90 min, then added to 500 µL (about 1 mg) whole cell lysates. Protein samples on PVDF membrane after transfer were washed four times with immunoprecipitation lysis/wash buffer overnight, then washed one time with condition buffer, and then eluted with solution buffer. The prepared samples were used for 12.5% SDS-PAGE electrophoresis and western blot. The samples were incubated with rabbit anti-mouse NMMHC **IIA** primary antibody (1:1000) and rabbit anti-mouse TLR4 primary antibody (1:1000) at 4 °C overnight, respectively. After TBST was washed three times, corresponding HRP-labeled antibodies were added and incubated for 1 h at room temperature. After TBST washing for three times, the images were captured by a Bio-Image Analysis System using ECL chemical solution. In addition, reverse co-immunoprecipitation and western blot is the same as above. Instead, the rabbit anti-mouse NMMHC **IIA** antibody was replaced by rabbit anti-mouse TLR4 antibody. The precipitated proteins carried out western blot with the same steps as previously described.

Animals and Cell Culture Grouping

In protocol 1, to determine regulation pattern of NMMHC IIA in tight junctions proteins in OGD-activated brain endothelial cells, we treated the cells with a myosin II inhibitor blebbistatin (Kovacs et al. 2004). NMMHC IIA-inhibited group was incubated with 1 µM blebbistatin for 1 h dissolved in DMSO. After the treatment of bEnd.3 endothelial cells, OGD was induced in the cells for 2 h in glucose-free RPMI

1640 medium in hypoxia chamber for 2 h, in an atmosphere of 5% CO_2 and 95% N_2, subsequently cultured under normoxia conditions. After pre-incubated with 1 μM blebbistatin for 1 h, the OGD + NMMHC IIA-inhibited group was obtained via the bEND.3 cells were then exposed to OGD for an additional 6 h. The control + vehicle group was treated with an equal volume of DMSO. The bEND.3 endothelial cells in each group were collected and applied to western blotting and immunofluorescence. The photos were taken using an Olympus Confocal Laser Scanning Microscope (Olympus, Nagano, Japan).

In protocol 2, to determine the regulation pattern of NMMHC IIA on tight junction in ischemia stroke, mice were pretreated with the NMMHC IIA inhibitor blebbistatin. C57BL/6 mice were anesthetized with 1.2% isoflurane during the ischemia period. Focal cerebral ischemia was carried out by intraluminal middle cerebral artery occlusion as previously described (Lv et al. 2015). A laser Doppler flowmeter (Moor Instruments, FLPI2, UK) was used to detect the blood flow of middle cerebral artery. Animals whose blood flow greater than 30% of pre-ischemia levels were used for further study. 6 mice were subjected to 2 h of ischemia stroke in the MCAO (Middle cerebral artery occlusion) model. The lysis solution was prepared from brain tissue of each group. The sham group received an equivalent volume of 0.9% NaCl solution. Mice were randomly divided into six groups ($n = 6$ in each group): (1) sham-operated mice; (2) MCAO mice exposed to 2 h of ischemia stroke; (3) C57BL/6J mice were injected with blebbistatin (1 mg/kg) intraperitoneally and then underwent 2 h of ischemia stroke later. At the end point of the ischemia stroke period, the brain tissues were executed for analysis of NMMHC IIA, occludin, claudin-5, ZO-1, and GAPDH expression. In addition, the tissue samples were immunostained and scanned by full electronic scanning, while the immunofluorescence of each brain specimen was examined by optical microscopy.

In protocol 3, in the inhibitor group, the inhibitor treatment was dissolved in DMSO and added 1 h prior to OGD stimulation, while cells in the control + vehicle group were treated with an equal volume of DMSO. The bEND.3 cells were randomly divided into five groups ($n = 9$ per group): (1) control + vehicle group; (2) OGD plus vehicle for 6 h; (3) pretreatment with low concentration inhibitor (The specific inhibitor and corresponding concentration were described in 2.8) and then exposed to OGD for 6 h; (4) pretreatment with moderate concentration inhibitor (The specific inhibitor and corresponding concentration were described in 2.8) and then exposed to OGD for 6 h; (5) pretreatment with high concentration inhibitor (The specific inhibitor and corresponding concentration were described in 2.8) and then exposed to OGD for 2 h. After 2 h of incubation, the bEND.3 cells in each group were collected and analyzed for NMMHC IIA, TLR4, p-PI3K, PI3K, p-Akt, Akt, p-JNK1/2, JNK1/2, p-Bad (S136), Bad (S136), p-Bad (S128), Bad (S128), 14-3-3ε, p-IKKα, IKKα, p-IKKβ, IKKβ, NF-κB p-p65, NF-κB p65, p-IκBα, IκBα, MMP9, occludin, claudin-5, ZO-1, and GAPDH expression via western blotting.

NMMHC IIA siRNA Transfection

bEND.3 endothelial cells were sub-cultured in 24-well plates with the density of 3×10^5 cells/mL. NMMHC IIA siRNA, and control non-specific siRNA were synthesized by Shanghai Biotechnology Corporation (CN). siRNA transfection was performed using ExFect Transfection Reagent (Shanghai Biotechnology Corporation, CN) according to the manufacturer's instructions. Cells were transfected with RNAs at a final concentration of 100 nM for 48 h. The NMMHC IIA sequences were: forward, 5-GAGGCAAUGAUCACUGAC UdTdT-3 and reverse, 5-AGUCAGUGAUCAUUGCCU CdTdT-3. To assess the NMMHC IIA siRNA efficiency, total NMMHC IIA siRNA cell lysate were subjected to western blot analysis, followed by GAPDH (Shanghai Biotechnology Corporation, CN) as internal reference.

Immunofluorescence of Related Proteins in bEND.3 Cells

To obtain green fluorescent protein (GFP) labeled bEND.3 cells were transducted with lentivirus harboring GFP generated using the Lenti-X HTX system (Daquinag et al. 2011), according to the manufacturer's protocol (Clontech, CN). According to protocol 1, bEND.3 cells were separately washed with phosphate-buffered saline (PBS, pH 7.4) and immobilized with cold ethanol at 4 °C for 10 min, and immobilized with 10% normal goat serum, 3% bovine serum albumin and 0.1% Triton X-100 in PBS for 1 h. Then incubated with the anti-NMMHC IIA (CST, USA, 3403, 1:1000 for WB, 1:50 for IF), anti-occludin (Invitrogen, USA, 33-1500, 1:1000 for WB, 1:200 for IF), anti-claudin-5 (Invitrogen, USA, 34-1600, 1:1000 for WB, 1:200 for IF), and anti-ZO-1 (Invitrogen, USA, 40-2300, 1:1000 for WB, 1:200 for IF) primary antibody for 48 h at 4 °C. After washing, cells separately were incubated overnight with Alexa Fluor® 488 conjugated Donkey Anti-Goat IgG (H + L) antibody (Abcam, UK, ab150129, 1:1000) at 4 °C. The wash step was repeated, the nuclei of all cells were then washed and incubated with 40,6-diamidino-2-phenylindole (DAPI, CST, USA, 4083, 1:1000) for 15 min at room temperature. Briefly, confocal images were converted to 8-bit format, and then noise speckle removal was performed to eliminate the single-pixel background fluorescence. The images were all converted to binary images and the fluorescence intensity in each group was analyzed of each frame.

Western Blot Analysis

The protein concentration was measured by the BCA assay. Samples containing 40 μg protein were isolated by 12.5% SDS-PAGE electrophoresis. Subsequently, the proteins were transferred onto PVDF membranes in Tris-glycine transfer buffer. The membranes were sealed with 5% nonfat dry milk for 2 h at room temperature. Rabbit anti-NMMHC IIA (CST, USA, 3403, 1:1000), anti-TLR4 (CST, USA, 14358, 1:1000), anti-p-PI3K (CST, USA, 4228(Tyr458), 1:1000), anti-PI3K (CST, USA, 4249, 1:1000), anti-p-Akt (CST, USA, 4060(Ser473), 1:1000), anti-Akt (CST, USA, 4685, 1:1000), anti-p-JNK1/2 (CST, USA, 9255(Thr183/Tyr185), 1:1000), anti-JNK1/2 (CST, USA, 9252, 1:1000), anti-p-Bad (S136) (CST, USA, 4366(Ser136), 1:1000), anti-Bad (S136) (CST, USA, 9292, 1:1000), anti-p-Bad (S128) (Abcam, UK, ab216829(Ser128), 1:1000), anti-Bad (S128) (CST, USA, 9292, 1:1000), anti-14-3-3ε (CST, USA, 9635, 1:1000), anti-p-IKKα/β (CST, USA, 2697(Ser176/180), 1:1000), anti-IKKα/β (CST, USA, 9936, 1:1000), anti-NF-κB p-p65 (CST, USA, 3033(Ser536), 1:1000), anti-NF-κB p65 (CST, USA, 4767, 1:1000), anti-p-IκBα (CST, USA, 2859(Ser32), 1:1000), anti-IκBα (CST, USA, 7543, 1:1000), anti-MMP9 (CST, USA, 3852, 1:1000) and anti-GAPDH (CST, USA, 5174, 1:1000) were applied to be incubated overnight, then incubated with the appropriate HRP-conjugated secondary antibody lasted for 50 min. The bands were displayed by enhanced chemiluminescence, while the images were captured by a Bio-Image Analysis System (Bio-Rad, Hercules, USA).

Double-Labeled Staining Evaluation of Albumin/Occludin, Albumin/Claudin-5, and Albumin/ZO-1

After ischemia stroke injury, the brains of protocol 2 mice were fixed with saline and infused with 4% paraformaldehyde for 24 h. After dehydration, the brains were embedded in paraffin and continuously cut into a series of 5-m thick section 20 μL FITC-albumin (Albumin-fluorescein isothiocyanate conjugate, Sigma-Aldrich, USA, A9771, 1:50) water solution (20 mg/ml FITC-albumin dissolved water solution) was applied to cover the brain section at 4 °C for 6 h. The sections were washed with PBS, and subjected to incubation with occludin (Invitrogen, USA, 33-1500, 1:200 for IF), claudin-5 (Invitrogen, USA, 34-1600, 1:200 for IF), and ZO-1 (Invitrogen, USA, 40-2300, 1:200 for IF) primary antibodies. Under 20 × objective using a 3-CCD color video camera, 9 fields of the ischemia boundary area were captured and analyzed[10]. Positive immunofluorescence staining area of occludin, claudin-5 and ZO-1 were measured under ×200 magnified view. The data were shown as the percentage of the positive stained area.

Detection of the NMMHC IIA-Mediated Pathway in OGD-Stimulated bEND.3 Endothelial Cells

We examined the effect of NMMHC IIA on the activity of tight junction-mediated pathway, in protocol 3, a dose-dependent inhibition experiment was used to test the regulation of the TJ-mediated pathway in OGD-stimulated bEND.3 endothelial cells. NMMHC IIA inhibitor blebbistatin (0.01, 0.1, 1 μM, respectively, for low, moderate, high dose)(Sigma-Aldrich, USA, B0560); TLR4 inhibitor TAK-242 (0.25 μM, 0.5 μM, 1 μM, respectively, for low, moderate, high dose)(Abmole, USA, M4838); PI3K/Akt inhibitor LY294002 (2.5, 5, 10 μM, respectively, for low, moderate, high dose)(Abmole, USA, M1925); JNK1/2 inhibitor SP600125 (10 20, 40 μM, respectively, for low, moderate, high dose)(Abmole, USA, M2076); 14-3-3 inhibitor R18 (25, 50, 100 μM, respectively, for low, moderate, high dose)(Generous gift from Department of Complex Prescription of TCM, China Pharmaceutical University); NF-κB inhibitor PDTC (50, 100 200 μM, respectively, for low, moderate, high dose)(Sigma, USA) (Abmole, USA, M4005); MMP9 inhibitor BB-1101 (10 20, 30 μM, respectively, for low, moderate, high dose) (Generous gift from Department of Complex Prescription of TCM, China Pharmaceutical University). MTT cell proliferation and cytotoxicity assay kit (Nanjing Jiancheng Bioengineering Institute, G020, CN) was applied to evaluate the cellular viability under OGD condition or not. Results from MTT assay made sure that the concentration chosen for each inhibitor did not affect cell viability. The bEND.3 cells in each group were subsequently collected and subjected to western blot analysis of NMMHC IIA, TLR4, p-PI3K, PI3K, p-Akt, Akt, p-JNK1/2, JNK1/2, p-Bad (S136), Bad (S136), p-Bad (S128), Bad (S128), 14-3-3ε, p-IKKα, IKKα, p-IKKβ, IKKβ, NF-κB p-p65, NF-κB p65, p-IκBα, IκBα, MMP9, occludin, claudin-5, ZO-1, and GAPDH expression. The use of antibodies was in accordance with the method in western blot assay.

Statistical Analysis

All values are expressed in terms of mean ± S.D. The data were analyzed by a two-tailed Student's *t* test (two groups) or two-way analysis of variance (ANOVA) followed by Bonferroni's test (three or more groups). The significance level was set at $P < 0.05$ and $P < 0.01$.

Results

Co-immunoprecipitation was used to Verify the Interaction Between NMMHC IIA and TLR4

Rabbit anti-mouse NMMHC IIA antibody and brain endothelial cell total protein were used for immunoprecipitation. The western blot results could detect TLR4 protein in immune complexes, and the bands appeared were consistent with those in total proteins of bEND.3 endothelial cells, which showed the authenticity of the results (Fig. 1). Correspondingly, the interaction between NMMHC IIA and TLR4 in bEND.3 endothelial cells was verified by reverse immunoprecipitation. The rabbit anti-mouse TLR4 antibody was used for reverse immunoprecipitation. Western blot could detect NMMHC IIA protein in immune complexes, and the bands appeared in western blot were consistent with the NMMHCIIA protein in total protein of bEND.3 endothelial cells (Fig. 1). This indicated that NMMHC IIA interacted with TLR4. And then the upstream and downstream relationship between the proteins were further investigated.

Inhibition of NMMHC IIA Improved Tight Junction Dysfunction in OGD-Stimulated bEND.3 Endothelial Cells and Ischemia Stroke Mice

Immunostaining and western blot analysis showed the activation of NMMHC IIA (red) in OGD-stimulated bEND.3 endothelial cells (OGD + vehicle: 1.72 ± 0.05, $P < 0.01$, control + vehicle: 1.07 ± 0.03, Fig. 2), while blebbistatin inhibited the upregulation expression of NMMHC IIA (1.37 ± 0.02, $P < 0.01$). Occludin, claudin-5, and ZO-1 were continuous and well organized in the bEND.3 cellular layer of microvessels in the control + vehicle group (Fig. 2). After stimulation with OGD, occludin, claudin-5, and ZO-1 revealed structural disruptions with re-arrangements compared with the control + vehicle group. The expression of occludin, claudin-5, and ZO-1 (0.64 ± 0.06, $P < 0.01$, 0.62 ± 0.01, $P < 0.01$, 0.70 ± 0.08, $P < 0.01$) were reduced compared with those the bEND.3 cells stimulated by OGD (1.12 ± 0.04, 1.17 ± 0.03, 1.21 ± 0.04, Fig. 2). Moreover, the fragmented immunocytochemical staining of TJ proteins along the bEND.3 cells border were restored to a brightener and more distinct shape in response to the inhibition of NMMHC IIA (occludin: 0.79 ± 0.02, $P < 0.01$; claudin-5: 0.82 ± 0.05, $P < 0.01$; ZO-1: 0.77 ± 0.03, $P < 0.01$, Fig. 2).

Endothelial cell injury of BBB could be evaluated by Evans Blue and albumin microvascular leakage (Garbuzova-Davis et al. 2013). The albumin/occludin, albumin/claudin-5, and albumin/ZO-1 double-labeled staining were observed for pathological changes in the ischemia hemisphere by immunofluorescence staining, respectively (Fig. 3). More leakage of FITC-albumin was seen in the ischemia area of ischemia hemisphere compared with that of the non-ischemia blood flow region. Fluorescence intensity of FITC-albumin in the ischemia area was reduced via the intervention of blebbistatin, thus possibly suggesting neurological recovery of ischemia-damaged area. This linear shape of tight junctions decreased after subjected to ischemia stroke, while the intensity of occludin, claudin-5, and ZO-1 signal was weaker compared with the sham group (Fig. 3). The results showed that blebbistatin could ameliorate the pathological damage of brain tissues, enhancing the signal intensity and improving immunostaining intensity of occludin, claudin-5, and ZO-1.

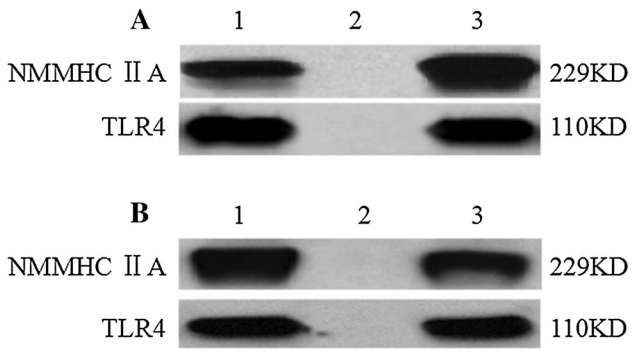

Fig. 1 Interaction between NMMHC IIA and TLR4 via co-immunoprecipitation was detected by western blot. **a** Western blot detected TLR4 protein in anti-NMMHC IIA co-immunoprecipitation complex. **b** Western blot detected NMMHC IIA protein in anti-TLR4 co-immunoprecipitation complex. (*1*): equal amount load sample of total bEND.3 endothelial cellular proteins; (*2*). co-immunoprecipitation with negative control; (*3*). specified protein obtained from anti-specified protein co-immunoprecipitation

Regulation of NMMHC IIA in OGD-Induced bEND.3 Endothelial Cells Influenced TLR4/PI3K/Akt/JNK1/2/14-3-3ε/NF-κB/MMP9 Pathways

Two-hour OGD not only upregulated the expression of NMMHC IIA, but also activated the expression of TLR4, p-PI3K, PI3K, p-Akt, Akt, p-JNK1/2, p-JNK1/2, p-Bad (S136), Bad (S136), p-Bad (S128), Bad (S128), 14-3-3ε, p-IKKα, IKKα, p-IKKβ, IKKβ, NF-κB p-p65, NF-κB p65, p-IκBα, IκBα, MMP9, occludin, claudin-5, and ZO-1. The myosin II inhibitor blebbistatin dose dependently (low, moderate, high dose: 1.59 ± 0.06, $P < 0.05$, 1.47 ± 0.04, $P < 0.05$, 1.36 ± 0.06, $P < 0.01$) suppressed the upregulation of NMMHC IIA (OGD + vehicle: 1.54 ± 0.03, $P < 0.01$), while TLR4 activation was prevented together with the phosphorylation of PI3K, Akt, JNK1/2, Bad (S136), Bad (S128), NF-κB p65, and 14-3-3ε at all protein levels (Fig. 4). The myosin II inhibitor blebbistatin dose dependently could also rescue the tight junction protein occludin (low, moderate,

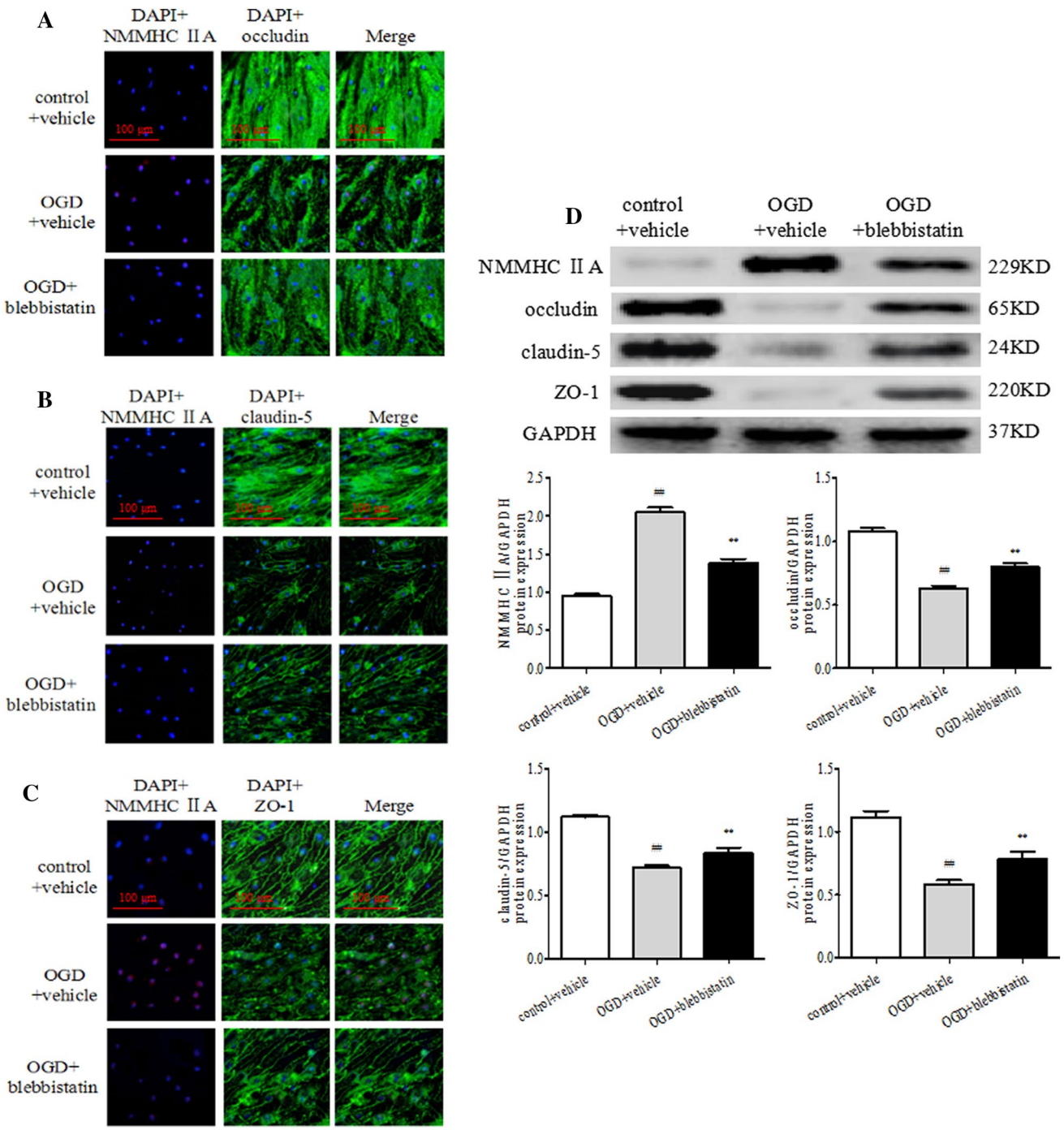

Fig. 2 The inhibition of NMMHC IIA on occludin, claudin-5, and ZO-1 expression in OGD-treated bEND.3 endothelial cells. **a**–**c**) Representative images on the colocalization of NMMHC IIA (red) and occludin (green), claudin-5 (green), and ZO-1 (green) in OGD-stimulated bEND.3 endothelial cells by immunofluorescent staining. The bEND.3 endothelial cells nuclei were counterstained with DAPI (blue). At a magnification of ×200, a confocal microscope is used to capture the images. The images were representative of nine individual plates from each group. **d** The expression of MMMHC IIA, occludin, claudin-5, and ZO-1 in OGD-treated bEND.3 endothelial cells was detected by western blot. The results were expressed as the percentage of control + vehicle from nine independent experiments. The data were averages with S.D., $n = 9$. $^{\#}P < 0.05$, $^{\#\#}P < 0.01$ vs. the control + vehicle group of bEND.3 endothelial cells, $^{*}P < 0.05$, $^{**}P < 0.01$ vs. the bEND.3 endothelial cells exposed to 2 h of OGD stimulation

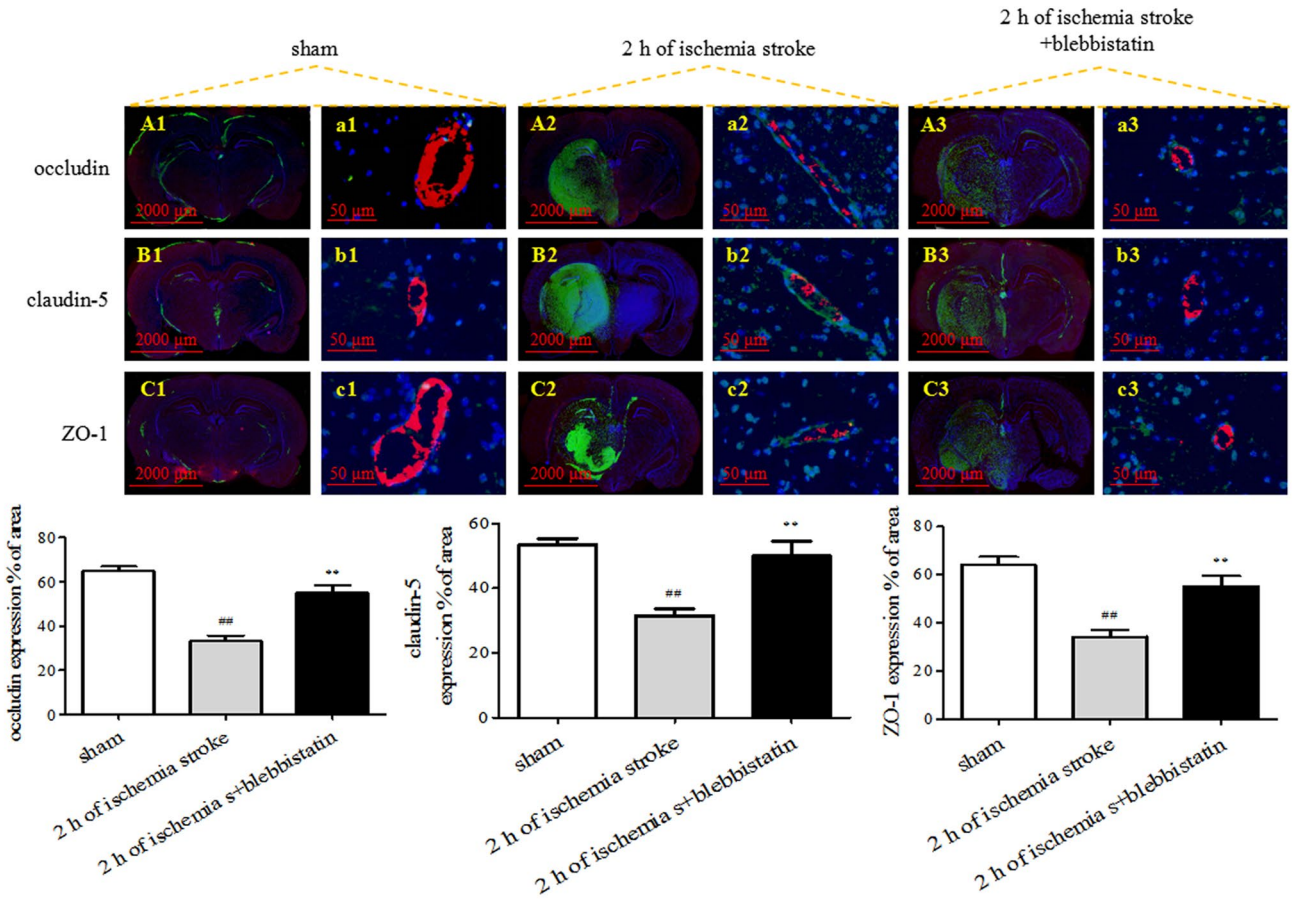

Fig. 3 The inhibiting effects of NMMHC IIA on the expression change in albumin/occludin, albumin/claudin-5, and albumin/ZO-1 in ischemia stroke mice via immunofluorescence staining. Six slides from each brain were digitized under a 20×objective with a 3-CCD color camera. Each slice contained eight fields of view from ischemia boundary region. Figures labeled with capital letters were the panoramic view of the figure. Throughout the scan, the figures labeled with lowercase letters of double-labeled staining of albumin (green)/occludin (red), albumin (green)/claudin-5 (red), and albumin (green)/ZO-1 (red) regions were observed under ×200 magnified view. The data were the percentage of positive cell numbers or positive vessel areas or areas in the ischemia boundary area. The results were expressed as six independent experiments. The data were averages with S.D., $n=6$. $^{\#}P<0.05$, $^{\#\#}P<0.01$ vs. sham mice, $^{*}P<0.05$, $^{**}P<0.05$ vs. 2 h of ischemia stroke mice

high dose: 0.48 ± 0.02, $P<0.01$, 0.53 ± 0.03, $P<0.01$, 0.66 ± 0.03, $P<0.01$; OGD + vehicle: 0.39 ± 0.05, $P<0.01$), claudin-5 (low, moderate, high dose: 0.49 ± 0.03, $P<0.01$, 0.53 ± 0.03, $P<0.01$, 0.67 ± 0.04, $P<0.01$; OGD + vehicle: 0.41 ± 0.02, $P<0.01$), and ZO-1 (low, moderate, high dose: 0.49 ± 0.04, $P<0.01$, 0.57 ± 0.05, $P<0.01$, 0.67 ± 0.06, $P<0.01$; OGD + vehicle: 0.40 ± 0.02, $P<0.01$). NMMHC IIA was successfully knocked down, which exhibited the significant descending change in protein expression. Furthermore, NMMHC IIA knockdown prevented the TLR4/PI3K/Akt/JNK1/2/14-3-3ε/NF-κB/MMP9 activation with or without OGD stimulation, which demonstrated a similar effect to the NMMHC IIA inhibitor blebbistatin (Fig. 5). These findings indicated that NMMHC IIA was the upstream role in regulating TLR4/PI3K/Akt/JNK1/2/14-3-3ε/NF-κB/MMP9 pathways. The suppression of NMMHC IIA expression could rescue the tight junction proteins in the OGD-stimulated bEND.3 endothelial cells.

The TLR4 inhibitor-TAK-242 had no effects on the upregulation of NMMHC IIA in OGD-stimulated bEND.3 endothelial cells, while TAK-242 dose dependently inhibited the activation of TLR4 and the phosphorylation of PI3K, Akt, JNK1/2, Bad (S136), Bad (S128), NF-κB p65, and 14-3-3ε in OGD-stimulated bEND.3 endothelial cells (Fig. 6). Subsequently, the cell groups subjected to the interference with PI3K inhibitor LY294002 revealed that the increased phosphorylation of PI3K and Akt were prevented by LY294002 (low, moderate, high dose, p-PI3K/PI3K: 1.64 ± 0.03, $P<0.05$, 1.50 ± 0.05, $P<0.05$, 1.43 ± 0.05, $P<0.01$; OGD + vehicle: 1.72 ± 0.05, $P<0.05$; p-Akt/Akt: 1.60 ± 0.07, $P<0.05$, 1.55 ± 0.07, $P<0.05$, 1.43 ± 0.01, $P<0.05$; OGD + vehicle: 1.64 ± 0.05, $P<0.01$) in a

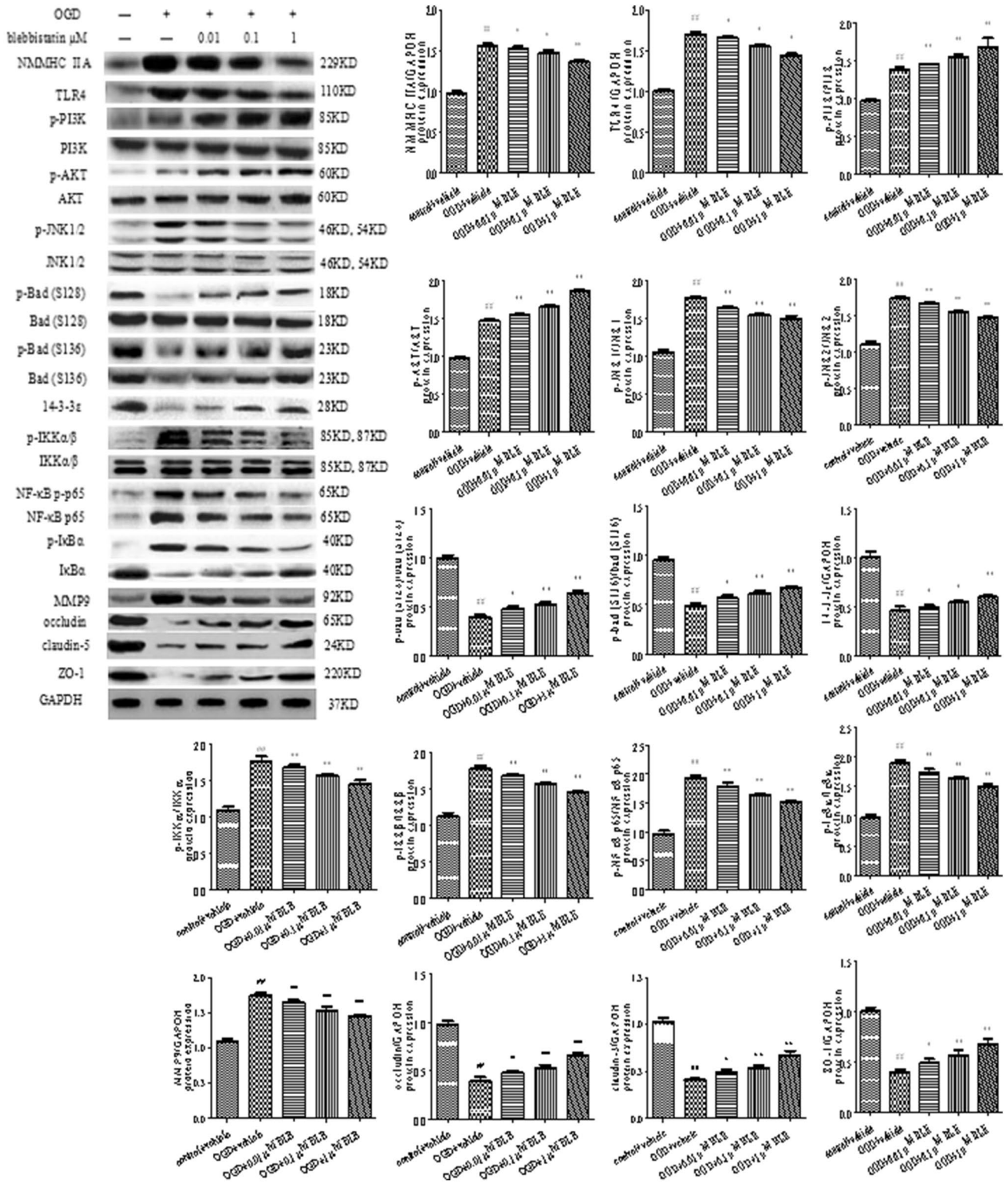

Fig. 4 Regulation of NMMHC IIA in OGD-treated bEND.3 endothelial cells influenced TLR4/PI3K/Akt/JNK1/2/14-3-3ε/NF-κB/MMP9 pathways and tight junction proteins. NMMHC IIA inhibitor blebbistatin was infused 1 h before OGD stimulation and subjected to an evaluation of the inhibitory effect on the TJ-mediated signaling pathway in bEND.3 endothelial cells via western blot analysis. The functions of NMMHC IIA inhibitor blebbistatin (0.01, 0.1, and 1 μM, respectively, for low, moderate, and high dose) were evaluated. Results were expressed as the percentage of control + vehicle from nine independent experiments. The data were averages with S.D., $n = 9$. $^{\#}P < 0.05$, $^{\#\#}P < 0.01$ vs. the control + vehicle group of bEND.3 endothelial cells, $^{*}P < 0.05$, $^{**}P < 0.01$ vs. the bEND.3 endothelial cells exposed to 2 h of OGD stimulation

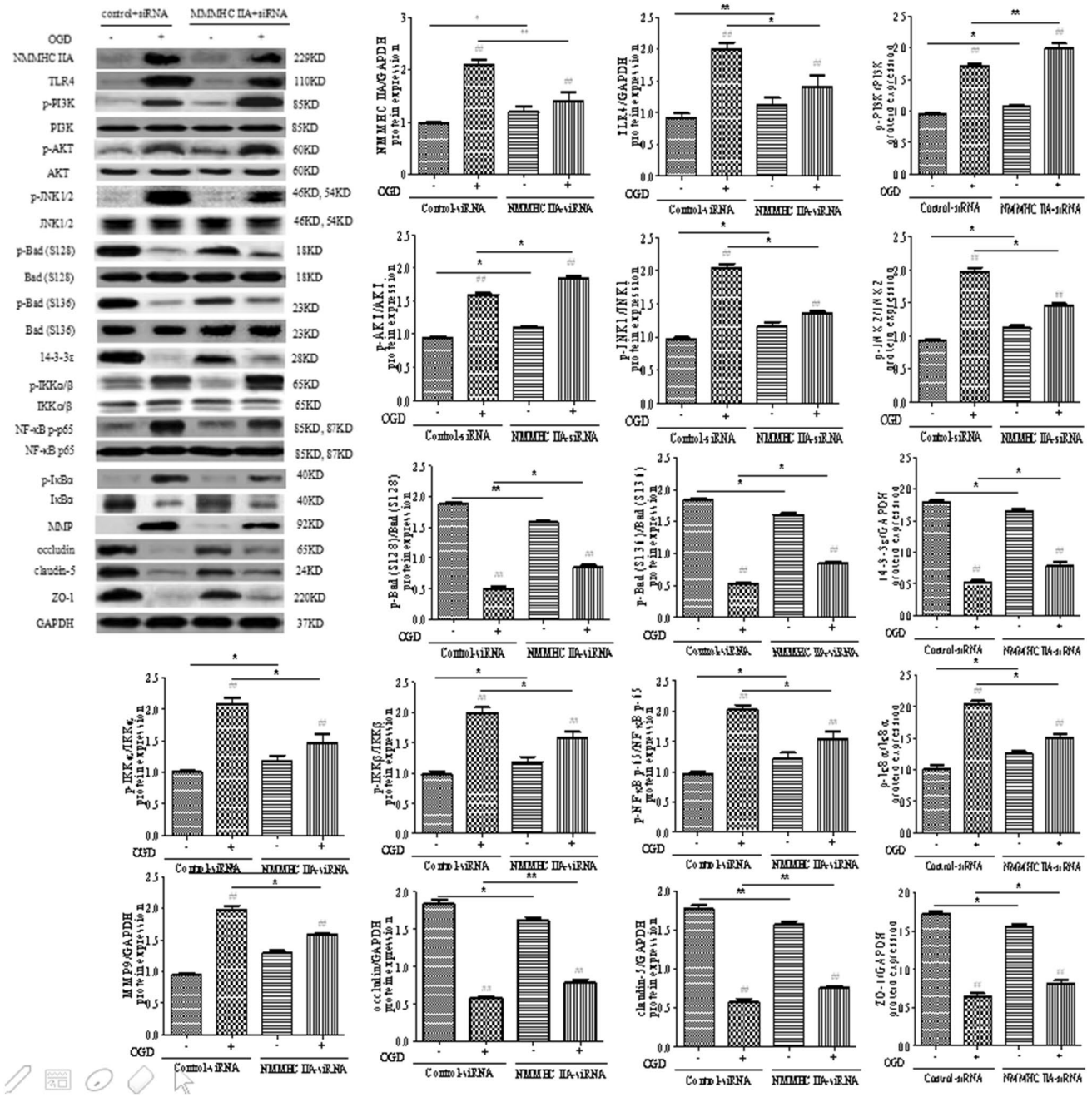

Fig. 5 The regulation of knockdown of NMMHC IIA on TLR4/PI3K/Akt/JNK1/2/14-3-3ε/NF-κB/MMP9 pathways and tight junction proteins in OGD-treated bEND.3 endothelial cells. After 48 h of transfection, control siRNA and NMMHC IIA knockdown bEND.3 cells were stimulated under OGD condition for 2 h. NMMHC IIA and total downstream targets were analyzed by western blotting. Results were expressed as the percentage of control + vehicle from nine independent experiments. The data were averaged with S.D., $n = 9$. $^{\#}P < 0.05$, $^{\#\#}P < 0.01$, vs. the control + siRNA or NMMHC IIA siRNA group of bEND.3 endothelial cells under OGD condition. $^{*}P < 0.05$, $^{**}P < 0.01$, the differences among three groups were analyzed by Bonferroni's test

dose-dependent manner, while the activation of NMMHC IIA and TLR4 showed no significant difference in comparison to the control + vehicle group (Fig. 7). Upregulation of p-JNK1/2, p-Bad (S136), p-Bad (S128), NF-κB p-p65 and downregulation of 14-3-3ε were inhibited. Moreover, dose-dependent inhibition of JNK1/2 by SP600125 (Fig. 8) affected the relative activity of p-JNK1/2 and p-Bad (S128) (low, moderate, high dose, p-JNK1/JNK1: 1.44 ± 0.07, $P < 0.05$, 1.39 ± 0.02, $P < 0.01$, 1.31 ± 0.04, $P < 0.01$; OGD + vehicle: 1.55 ± 0.06, $P < 0.01$; p-JNK2/JNK2: 1.44 ± 0.02, $P < 0.05$, 1.37 ± 0.02, $P < 0.05$, 1.31 ± 0.06, $P < 0.05$; OGD + vehicle: 1.57 ± 0.07, $P < 0.01$; p-Bad

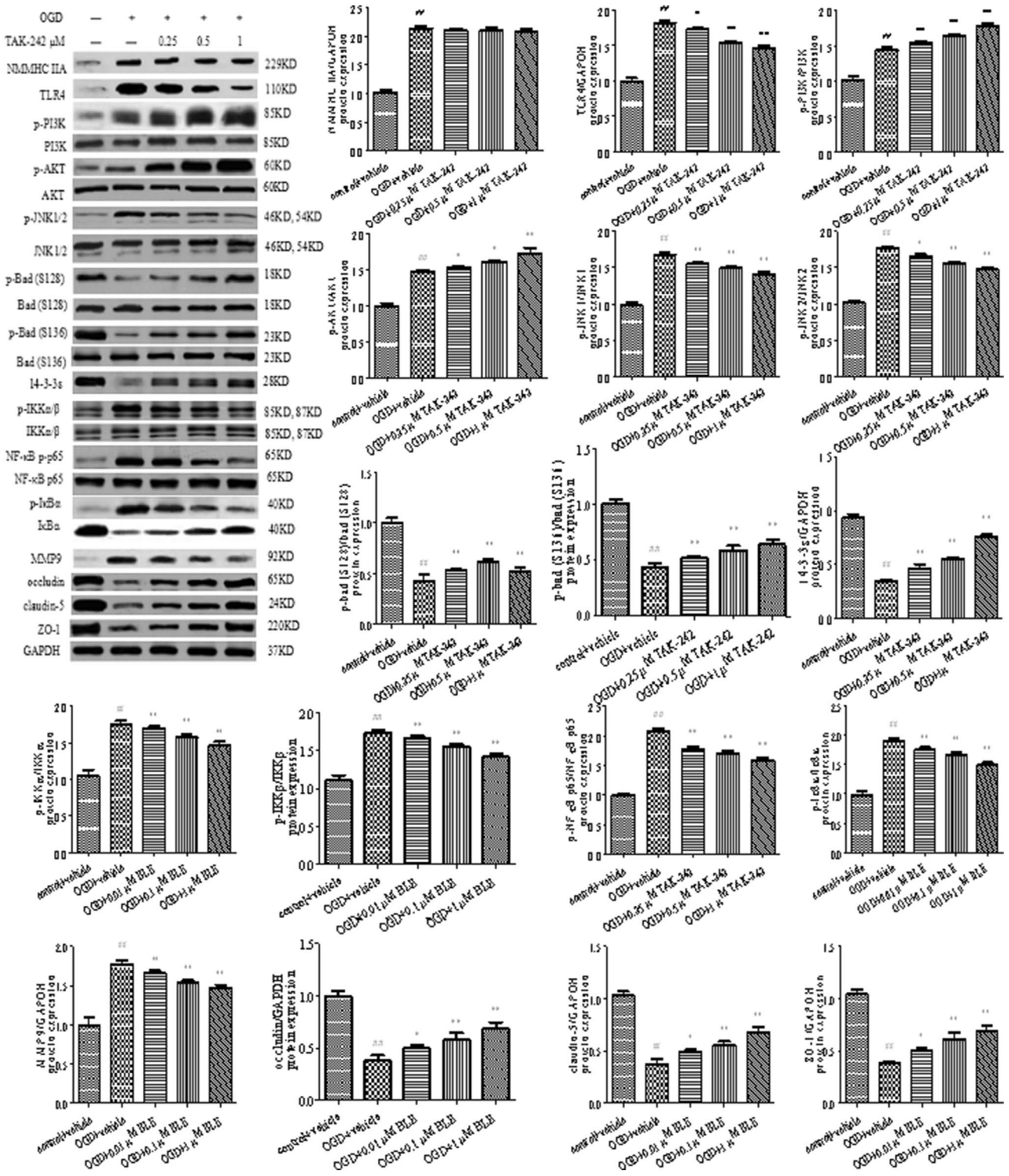

Fig. 6 Regulation of TLR4 in OGD-treated bEND.3 endothelial cells influenced PI3K/Akt/JNK1/2/14-3-3ε/NF-κB/MMP9 pathways and tight junction proteins. TLR4 inhibitor-TAK-242 was infused 1 h before OGD stimulation and subjected to an evaluation of the inhibitory effect on the TJ-mediated signaling pathway in bEND.3 endothelial cells via western blot analysis. The functions of TLR4 inhibitor-TAK-242 (0.25 μM, 0.5 μM, and 1 μM, respectively, for low, moderate, and high dose) were evaluated. Results were expressed as the percentage of control + vehicle from nine independent experiments. The data were averages with S.D., $n = 9$. $^{\#}P < 0.05$, $^{\#\#}P < 0.01$ vs. the control + vehicle group of bEND.3 endothelial cells, $^{*}P < 0.05$, $^{**}P < 0.01$ vs. the bEND.3 endothelial cells exposed to 2 h of OGD stimulation

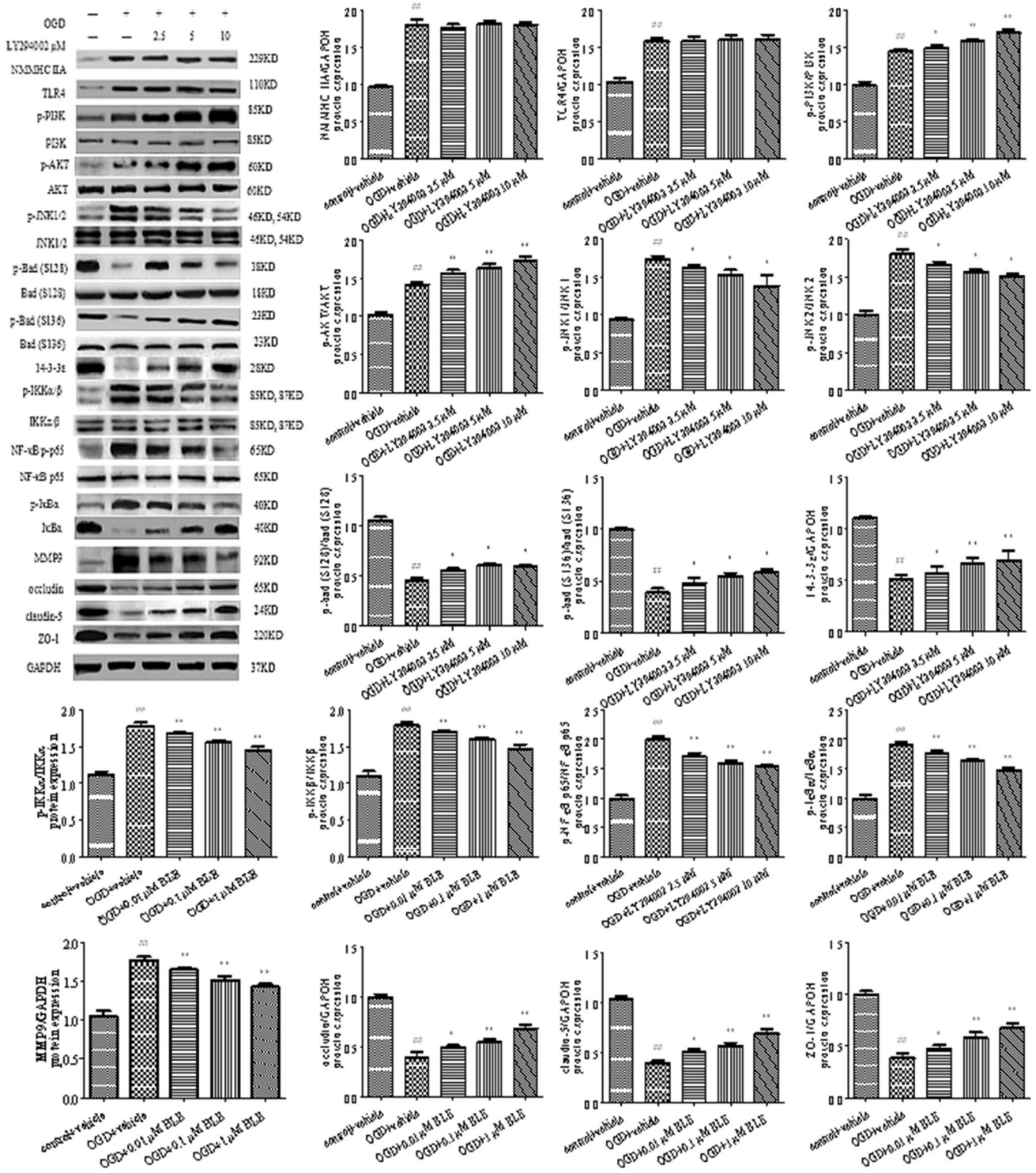

Fig. 7 Regulation of PI3K/Akt in OGD-treated bEND.3 endothelial cells influenced JNK1/2/14-3-3ε/NF-κB/MMP9 pathways and tight junction proteins. PI3K/Akt inhibitor-LY294002 was infused 1 h before OGD stimulation and subjected to an evaluation of the inhibitory effect on the TJ-mediated signaling pathway in bEND.3 endothelial cells via western blot analysis. The functions of PI3K/Akt inhibitor-LY294002 (2.5, 5, and 10 μM, respectively, for low, moderate, and high dose) were evaluated. Results were expressed as the percentage of control + vehicle from nine independent experiments. The data were averages with S.D., $n=9$. $^{\#}P<0.05$, $^{\#\#}P<0.01$ vs. the control + vehicle group of bEND.3 endothelial cells, $^{*}P<0.05$, $^{**}P<0.01$ vs. the bEND.3 endothelial cells exposed to 2 h of OGD stimulation

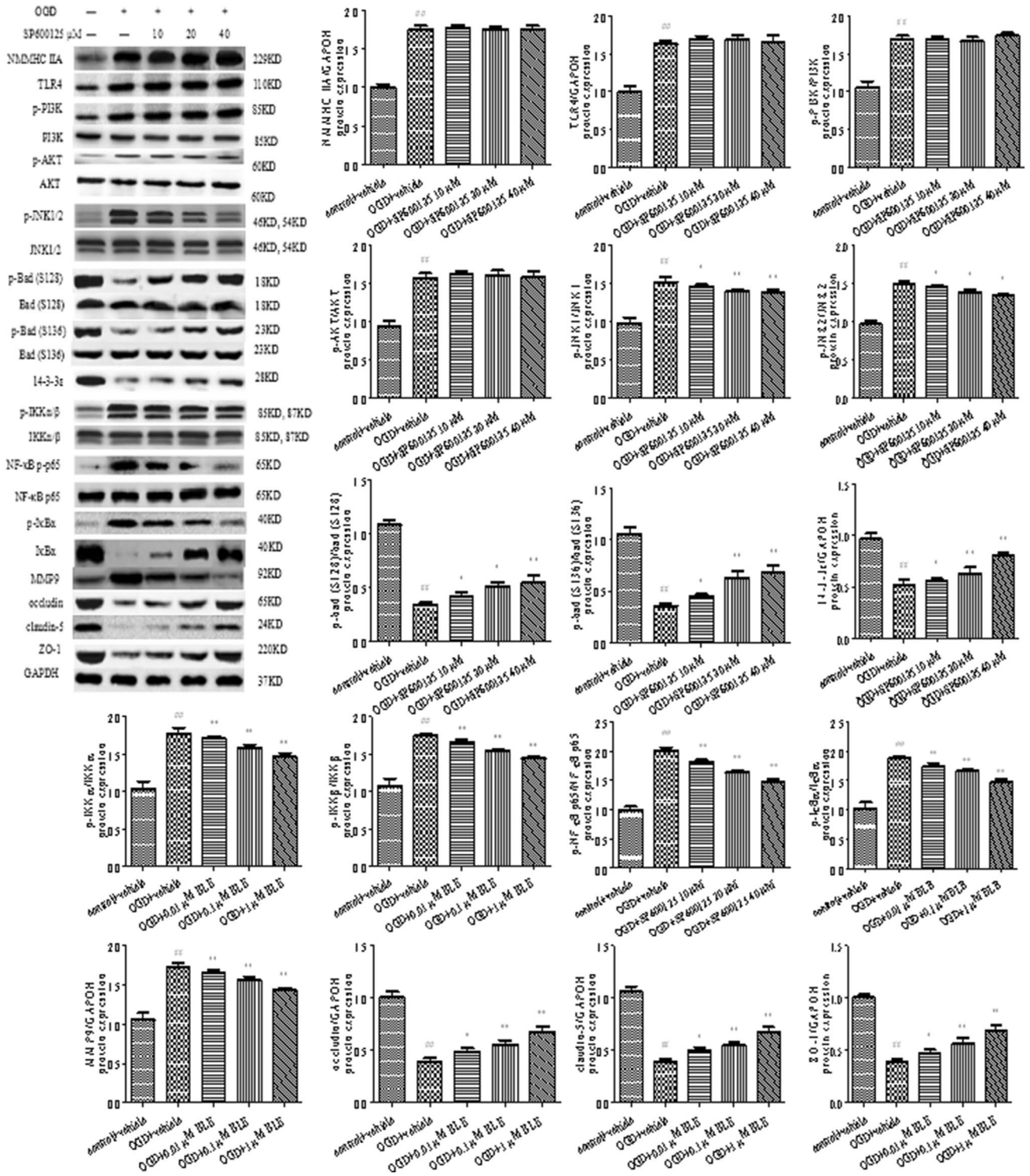

Fig. 8 Regulation of JNK1/2 in OGD-treated bEND.3 endothelial cells influenced 14-3-3ε/NF-κB/MMP9 pathways and tight junction proteins. JNK1/2 inhibitor-SP600125 was infused 1 h before OGD stimulation and subjected to an evaluation of the inhibitory effect on the TJ-mediated signaling pathway in bEND.3 endothelial cells via western blot analysis. The functions of JNK1/2 inhibitor-SP600125 (10 20, and 40 μM, respectively, for low, moderate, and high dose) were evaluated. Results were expressed as the percentage of control + vehicle from nine independent experiments. The data were averages with S.D., $n = 9$. $^{\#}P < 0.05$, $^{\#\#}P < 0.01$ vs. the control + vehicle group of bEND.3 endothelial cells, $^{*}P < 0.05$, $^{**}P < 0.01$ vs. the bEND.3 endothelial cells exposed to 2 h of OGD stimulation

(S128)/Bad (S128): 0.41 ± 0.02, $P < 0.05$, 0.56 ± 0.06, $P < 0.05$, 0.64 ± 0.07, $P < 0.01$; OGD + vehicle: 0.33 ± 0.06, $P < 0.01$), while the expression of NMMHC IIA and TLR4, and the phosphorylation of PI3K, Akt, Bad (S136), and NF-κB P65 were not influenced. Interestingly, the phosphorylation of Bad (S136) was inhibited only by PI3K/Akt inhibitor-LY294002, however, had no influence of the inhibition of JNK1/2 inhibitor-SP600125, while 14-3-3ε were still downregulated and inhibited by either one of the inhibitors. The activation of TLR4 and the phosphorylation of PI3K, Akt, JNK1 and JNK2 were blocked by a high dose of the 14-3-3 inhibitor-R18, while the phosphorylation of Bad (S136)/Bad (S128), 14-3-3ε, phosphorylation of IKKα/β/NF-κB p-p65/IκBα, and MMP9 were blocked by all doses of the 14-3-3 inhibitor-R18, whereas NMMHC IIA was not affected (Fig. 9). All the mentioned inhibitors could restore the decreased expression of occludin, claudin-5, and ZO-1 tight junctions.

Pyrrolidine dithiocarbamate (PDTC), a metal chelator and antioxidantis, a selective NF-κB inhibitor, which could inhibit the activation of NF-κB specifically by suppressing the release of the inhibitory subunit IκB from the latent cytoplasmic form of NF-κB. In contrast to other inhibitors, treatment with the NF-κB inhibitor PDTC had no effect on other proteins except for the phosphorylation of NF-κB pathway itself and MMP9, p-IKKα/IKKα (low, moderate, high dose: 1.43 ± 0.04, $P < 0.01$, 1.56 ± 0.04, $P < 0.01$, 1.69 ± 0.04, $P < 0.01$; OGD + vehicle: 1.80 ± 0.06, $P < 0.01$), p-IKKβ/IKKβ (low, moderate, high dose: 1.67 ± 0.02, $P < 0.01$, 1.56 ± 0.03, $P < 0.01$, 1.43 ± 0.04, $P < 0.01$; OGD + vehicle: 1.79 ± 0.06, $P < 0.01$), p-IκBα/IκBα (low, moderate, high dose: 1.75 ± 0.03, $P < 0.01$, 1.64 ± 0.03, $P < 0.01$, 1.44 ± 0.05, $P < 0.01$; OGD + vehicle: 1.86 ± 0.02, $P < 0.01$), p-NF-κB p65/NF-κB p65 (low, moderate, high dose: 1.57 ± 0.04, $P < 0.05$, 1.51 ± 0.05, $P < 0.01$, 1.44 ± 0.04, $P < 0.01$; OGD + vehicle: 1.73 ± 0.03, $P < 0.01$), and MMP9 (low, moderate, high dose: 1.63 ± 0.03, $P < 0.01$, 1.52 ± 0.06, $P < 0.01$, 1.41 ± 0.04, $P < 0.01$; OGD + vehicle: 1.75 ± 0.05, $P < 0.01$) (Fig. 10). Different concentrations of MMP9 inhibitor BB-1101 could only affect MMP9 itself (low, moderate, high dose: 1.64 ± 0.04, $P < 0.01$, 1.52 ± 0.05, $P < 0.01$, 1.40 ± 0.04, $P < 0.01$; OGD + vehicle: 1.77 ± 0.07, $P < 0.01$), simultaneously could rescue the decreasing change of tight junction proteins (Fig. 11).

Discussion

The TJ transmembrane proteins included intact membrane proteins, such as the occludin, claudins, and zonula occludens, which were identified as inducing the formation of TJ-like structures (Wen et al. 2004). TJ proteins of the BBB were considered to be new insights into function and dysfunction disorders, suggesting that paraendothelial transport mediated by TJ participated in endothelial cell-mediated BBB permeability. The executive phase of TJ protein variation was characterized by a variety of morphological changes. It has been shown to regulate the BBB permeability and to induce loss of occludin, claudin-5, and ZO-1 tight junction proteins. In addition, many studies have shown that the increase in permeability of BBB marked the degradation of ZO-1 and other closely coupled components (Liu et al. 2012). The fluorescence in endothelial cell microvessels was shown with a significant decrease in occludin, claudin-5, and ZO-1 intensity under OGD condition. There was a trend toward increased occludin, claudin-5, and ZO-1 fluorescence in the NMMHC IIA inhibition group. In addition, immunofluorescence suggested that the bEND.3 endothelial cells structure were recovered with a more dense neuropil and tight boundary connection tight junction. The maintenance of tight junctions depended on the proper tissues of connective scaffold proteins such as ZO-1, therefore it was expected that TJ would be interrupted due to the alters in contraction patterns.

GO analysis and KEGG pathway in our previous work indicated that the original role of NMMHC IIA in the ischemia stroke mice displayed a close connection with tight junction of BBB (Lv et al. 2018). MYH9 was recruited to cell attachment and protein binding GO ontology annotation, and TJ signal KEGG pathways (Lv et al. 2018). Recent reports have revealed that the maintenance of epithelial barrier depended on the proper assembly of the actin cytoskeleton and intercellular junctions (Campos et al. 2016). Research examining intestinal mucosal barrier permeability has indicated that non-muscle myosin II was a key cytoskeletal motor for the integrity of epithelial TJs (Naydenov et al. 2016). It is known that actin–myosin cytoskeleton that generated contractile force, which is the main mechanism promoting cellular morphological changes and cellular apoptosis (Kim et al. 2015). Activation of myosin light chain kinase could increase the assembly of non-muscle myosin II and mediate the role of proinflammatory signals in simple epithelia and in TJ tissues (Turner et al. 2006). Myosin IIA was reported to bind to actin more quickly and strongly than myosin IIB (Kolega et al. 2006). The interaction between myosin IIA and F-actin provided the basis for H_2O_2-induced contractile forces in neuronal cells (Wang et al. 2016a, b). In addition, researches have showed that knocking down NMMHC IIA, but not NMMHC IIB or NMMHC IIC, significantly reduced the levels of TF protein in TNF-stimulated endothelial cells, while NMMHC IIA was likely located upstream of Akt/GSK3β-NF-κB based on its regulation of the signaling pathways (Zhai et al. 2015). Meanwhile, NMMHC IIA-activated PI3K-AKT signaling following MEK inhibition in metastatic negative breast cancer (Choi et al. 2016), while it could inhibit migration and invasion of

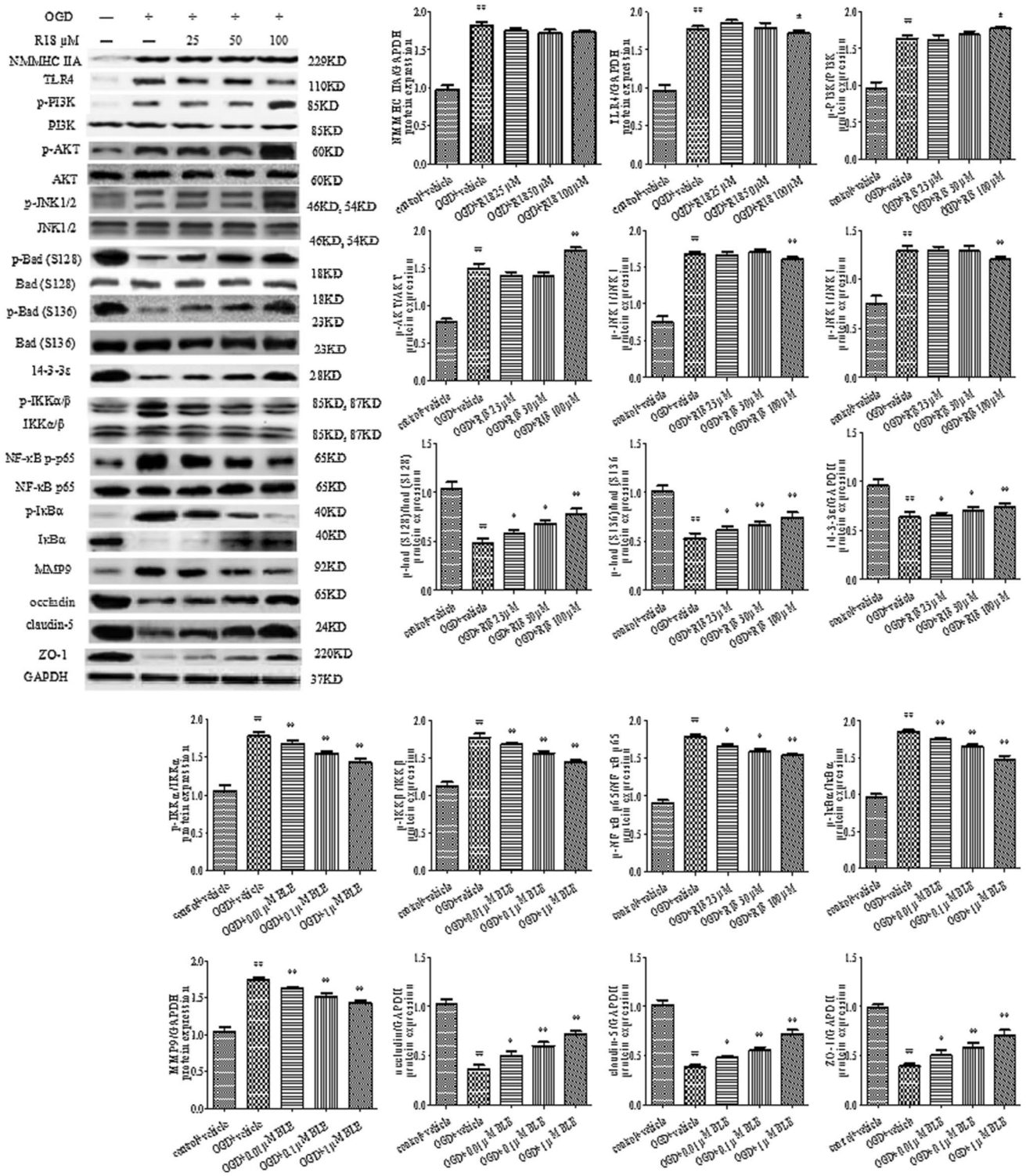

Fig. 9 Regulation of 14-3-3ε in OGD-treated bEND.3 endothelial cells influenced TLR4/PI3K/Akt/JNK1/2/14-3-3ε/NF-κB/MMP9 pathways and tight junction proteins. 14-3-3 inhibitor-R18 was infused 1 h before OGD stimulation and subjected to an evaluation of the inhibitory effect on the TJ-mediated signaling pathway in bEND.3 endothelial cells via western blot analysis. The functions of 14-3-3 inhibitor-R18 (25, 50, and 100 μM, respectively, for low, moderate, and high dose) were evaluated. Results were expressed as the percentage of control + vehicle from nine independent experiments. The data were averages with S.D., $n = 9$. $^{\#}P < 0.05$, $^{\#\#}P < 0.01$ vs. the control + vehicle group of bEND.3 endothelial cells, $^{*}P < 0.05$, $^{**}P < 0.01$ vs. the bEND.3 endothelial cells exposed to 2 h of OGD stimulation

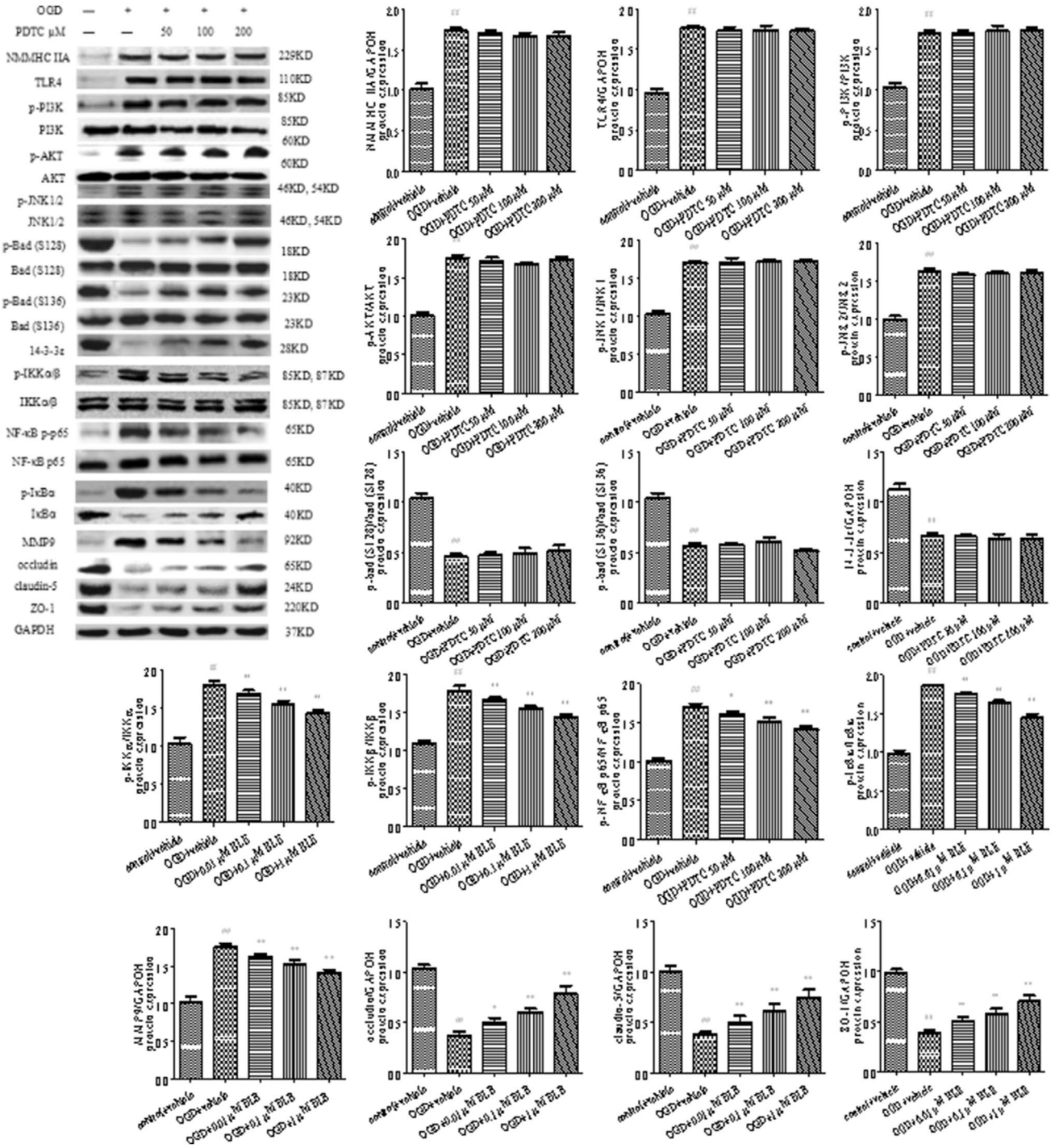

Fig. 10 Regulation of NF-κB p65 in OGD-treated bEND.3 endothelial cells influenced 14-3-3ε/NF-κB/MMP9 pathways and tight junction proteins. NF-κB inhibitor PDTC was infused 1 h before OGD stimulation and subjected to an evaluation of the inhibitory effect on the TJ-mediated signaling pathway in bEND.3 endothelial cells via western blot analysis. The functions of NF-κB inhibitor-PDTC (50, 100, and 200 μM, respectively, for low, moderate, and high dose) were evaluated. Results were expressed as the percentage of control + vehicle from nine independent experiments. The data were averaged with S.D., $n = 9$. $^{\#}P < 0.05$, $^{\#\#}P < 0.01$ vs. the control + vehicle group of bEND.3 endothelial cells, $^{*}P < 0.05$, $^{**}P < 0.01$ vs. the bEND.3 endothelial cells exposed to 2 h of OGD stimulation

gastric cancer cells via the c-Jun N-terminal kinase signaling pathway (Liu et al. 2016). Our data demonstrated that disruption of tight junctions between bEND.3 endothelial cells was mediated through activation of NMMHC IIA by inhibition test. The data demonstrated that treatment with myosin II inhibitor blebbistatin suppressed the activation

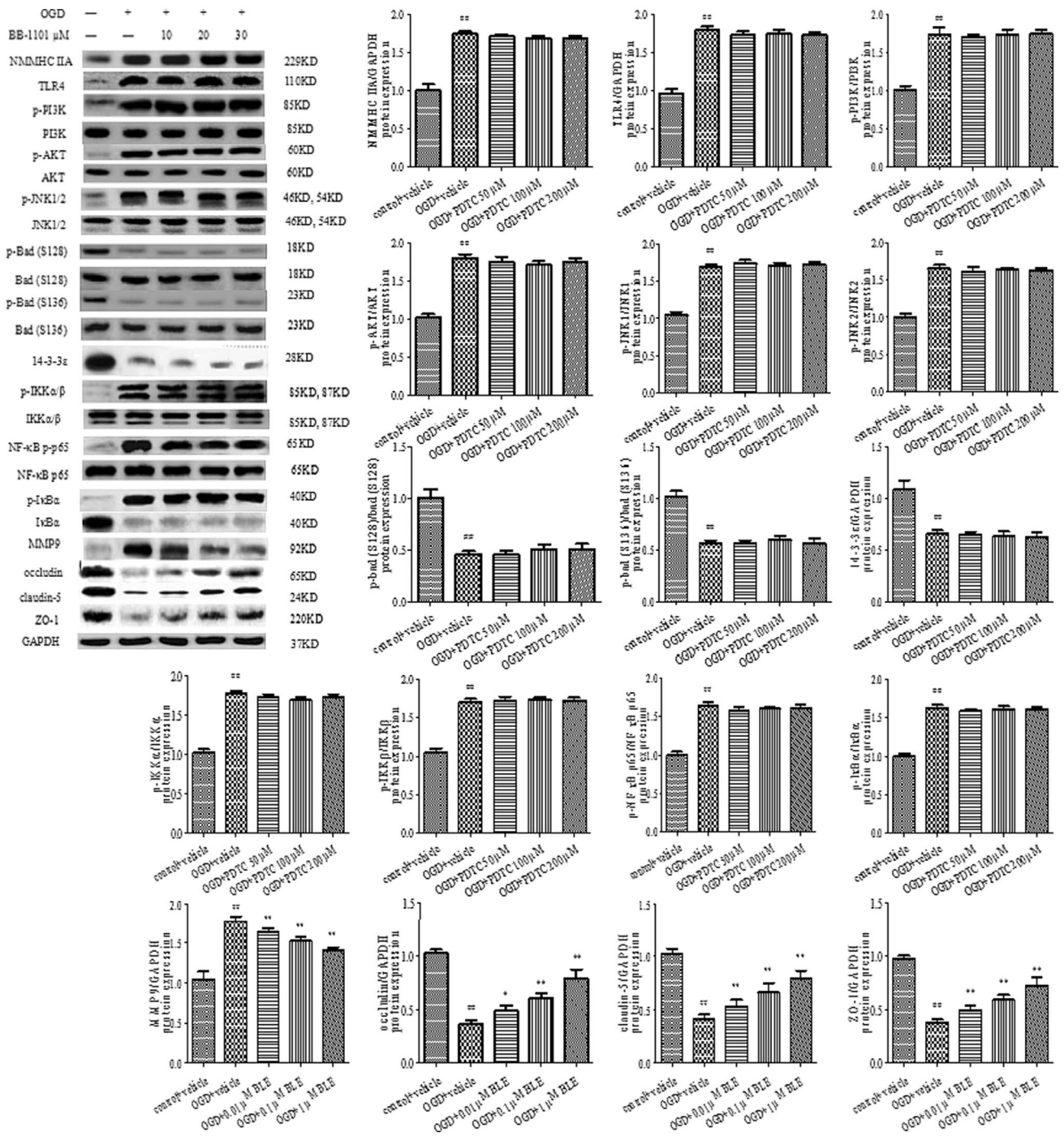

Fig. 11 Regulation of MMP9 in OGD-treated bEND.3 endothelial cells influenced and tight junction proteins. MMP9 inhibitor BB-1101 was infused 1 h before OGD stimulation and subjected to an evaluation of the inhibitory effect on the TJ-mediated signaling pathway in bEND.3 endothelial cells via western blot analysis. The functions of MMP9 inhibitor-BB-1101 (10 20, and 30 μM, respectively, for low, moderate, and high dose) were evaluated. Results were expressed as the percentage of control + vehicle from nine independent experiments. The data were averages with S.D., $n = 9$. $^{\#}P < 0.05$, $^{\#\#}P < 0.01$ vs. the control + vehicle group of bEND.3 endothelial cells, $^{*}P < 0.05$, $^{**}P < 0.01$ vs. the bEND.3 endothelial cells exposed to 2 h of OGD stimulation

of TLR4 together with the phosphorylation of PI3K, Akt, JNK1/2, Bad (S136), Bad (S128), 14-3-3ε, NF-κB, and MMP9 at all protein levels. In addition, in the inhibition of TLR4, PI3K, Akt, JNK1/2, Bad (S136), Bad (S128), NF-κB p65, 14-3-3ε, NF-κB or MMP9 could not produce any effect on the expression of NMMHC IIA, which confirmed the

upstream NMMHC IIA regulation of PI3K/Akt/JNK1/2/14-3-3ε/NF-κB/MMP9 activation. According to our results, our results provided evidences for the central role of NMMHC IIA in mediating TLR4-mediated signaling pathways in OGD-stimulated bEND.3 endothelial cells.

TLR4 was induced in response to a strong inflammatory response to BBB dysfunction and brain edema following focal cerebral ischemia (Cai et al. 2016). Meanwhile, inhibition of the PI3K/Akt/Rac-1 signaling pathway underlied the protective role in the regulation of TJ protein BBB. MAPK/ERK and PI3K/Akt kinase pathways were involved in the regulation of BBB permeability and the early nuclear translocation of NF-κB (Wang et al. 2016a, b). It was suggested that the TJ pathway was closely related to either TLR4 or PI3K/Akt signaling pathways. Koch's postulates were used in this study to interpret the relationships via the gradual addition of corresponding inhibitors. After interference with TLR4 inhibitor, the expressions levels of PI3K, Akt, JNK1/2, Bad (S136), Bad (S128), NF-κB p65, and 14-3-3ε were altered, which might be triggered by common upstream signals. Subsequent exposure to the PI3K inhibitor, p-Akt and p-JNK1/2 were both influenced. The literature also indicated that PI3K/Akt/FoxO1 signaling pathway was shown to participate in OGD-induced TLR4 expression and microglial activation (Zhaocheng et al. 2016). Meanwhile, we found that the increased phosphorylation of PI3K, Akt and JNK1/2 exerted the functions on p-Bad (S136), p-Bad (S128), 14-3-3ε, and NF-κB p-p65. These results demonstrated the PI3K/Akt could regulate the JNK1/2/14-3-3ε/NF-κB pathways in OGD-stimulated bEND.3 endothelial cells. Moreover, 14-3-3 had been shown to participate in the formation of TLR-mediated signaling platform (Funami et al. 2016). Reports have been reported that 14-3-3ε and 14-3-3σ could impair TLR4-mediated NF-κB and IFN-β reporter gene activity, and also bind to TLR aptamers (Butt et al. 2014). Meanwhile, the cellular process of autophagy adjusted by MAPK, PI3K, and mTOR were tightly regulated by 14-3-3 proteins (Pozuelo-Rubio et al. 2012). Furthermore, 14-3-3ζ enhanced Akt phosphorylation by activating PI3K bound to the p85 regulatory subunit of PI3K and increasing PI3K transport to the cell membrane (Neal et al. 2012). In the present study, 14-3-3 could reduce the relative activity of TLR4, PI3K, Akt, JNK1 and JNK2, which could regulate the TLR4/PI3K/Akt/JNK1/2 pathways in both positive and negative patterns. The potential mechanisms of occludin degradation could be due to MMP9. Occludin were degraded by MMP9 and rescued by MMP inhibitor BB-1101 after focal cerebral ischemia (Liu et al. 2009). MMP9 was confirmed to be modulated Akt/NF-κB pathway (Lu et al. 2018) or JNK-p38-ERK signaling pathway (Zhou et al. 2017). A possible mechanism, according to the results of sequence added corresponding inhibitor was shown in Fig. 12.

14-3-3ε is a member of the 14-3-3 protein family, which acted as an anti-apoptotic role by isolating pro-apoptotic molecules such as Bad (Schuster et al. 2011). Phosphorylated Bad interacts with 14-3-3, which prevents Bad from interacting with Bcl-xl on mitochondrial membrane (Wu et al. 2009). In the present study, under OGD condition, both p-Bad (S136), and p-Bad (S128) were activated, while 14-3-3ε expression was inhibited. Inhibition of PI3K/Akt influenced the activity of p-JNK1/2, and the activity of p-Bad (S136), p-Bad (S128), and 14-3-3ε. The downregulation of p-Bad (S136) and p-Bad (S128) displayed the same tendency, with a reduction of 14-3-3ε leading to reduced binding. This result was consistent with the literature (Zhu et al. 2014; Nomura et al. 2003), might be due to potential regulation of JNK1/2 by PI3K/Akt. Increasing evidence suggested that Bad could be phosphorylated not only by Akt1 but also by JNK1/2 after transient global ischemia in the rat hippocampal CA1 region (Wang et al. 2007). Akt1 mediated the phosphorylation of Bad at serine 136, leading to neuronal survival. In contrast, JNK1/2 induced the phosphorylation

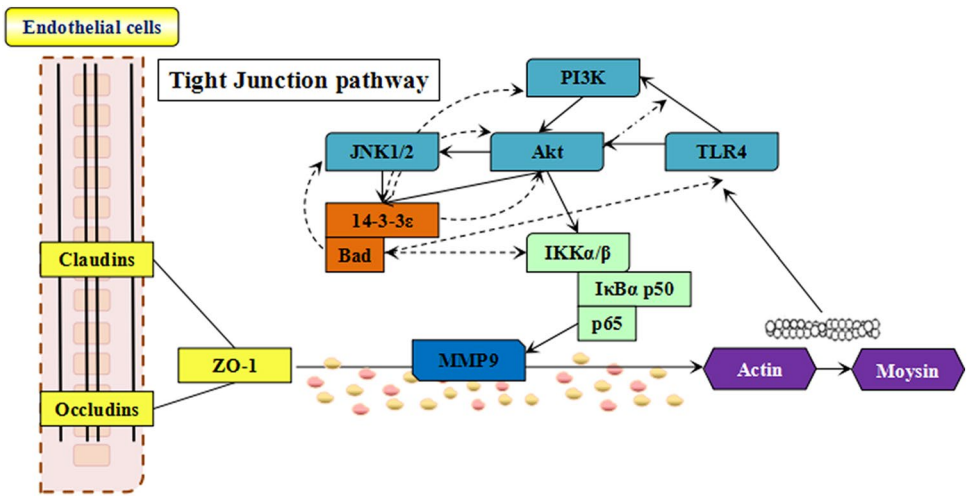

Fig. 12 Schematic representation of the role of NMMHC IIA in the regulation of tight junction in OGD-stimulated bEND.3 endothelial cells

of Bad at serine 128, inhibiting the interaction of PI3K/Akt-induced serine 136-phosphorylated Bad with 14-3-3 proteins and thereby promoting the apoptotic effect of Bad. The fate of cells to survive or die depended on a balance between survival and apoptotic signals. Inhibition of JNK1/2 under OGD-treated bEND.3 cells led to the upregulation of Bad (S128) phosphorylation, with no influence on the activity of p-Bad (S136), while the total expression tendency of 14-3-3ε was still downregulated. PI3K/Akt and JNK1/2 was affected by the balance of 14-3-3ε, while JNK1/2 played a critical role in bEND.3 cells under OGD condition, further improving the survival rate of apoptotic cells.

Although efforts have been made to ensure the interlinks of signaling pathways as complete as possible, more accurate experimental methods such as siRNA, co-immunoprecipitation, in situ hybridization deed need to be subjected to in-depth exploration. This study offered a promising explanation for interpreting the role of NMMHC IIA underlying BBB dysfunction induced by ischemia stroke via the TLR4/PI3K/Akt/JNK1/2/14-3-3ε/NF-κB/MMP9 pathway. Further elucidating the pathological process of ischemia stroke required more comprehensive potential targets and signaling pathways.

Conclusions

Our findings uncovered a key role of NMMHC IIA in modulating tight junction dysfunction mediated by regulating TLR4/PI3K/Akt/JNK1/2/14-3-3ε/NF-κB/MMP9 signaling pathways. These results provided compelling evidence for the role of NMMHC IIA in ischemia stroke and might lead to novel therapeutics for cerebral ischemia-related diseases.

Acknowledgements This work was supported by Foundation Project: National Natural Science Foundation of China (81760094, 31602111, 81860020), China; Jiangxi Provincial Education Department Science and Technology Research Youth Project (No. GJJ160238); The Foundation of Jiangxi Provincial Department of Science and Technology Youth Project (No. 20171BAB215021). The funder has no role in the study design, data collection and analysis, decision to publish or preparation of the manuscript.

Author Contributions All authors contributed to the research. YL conceived the experiments. YL, WL, ZR, ZX, LF conducted the experiments and analyzed the results. All authors contributed to the writing and editing of the manuscript.

Compliance with Ethical Standards

Conflict of interest None of the authors have any conflicts of interest, including financial, personal or other relationships, with other individuals or organizations.

Ethical Approval All animal care and experimental procedures were conducted according to standard ethical guidelines (National Institutes of Health Guide to the use of Laboratory Animals) and approved by Institutional Animal Care and use Committee of Nanchang University. All efforts were made to minimize the number of mice used and their suffering.

References

Butt T, Mufti T, Humayun A, Rosenthal PB, Khan S, Khan S et al (2010) Myosin motors drive long range alignment of actin filaments. J Biol Chem 285:4964–4974

Butt AQ, Ahmed S, Maratha A, Miggin SM (2014) 14-3-3ε and 14-3-3σ inhibit Toll-like receptor (TLR)-mediated proinflammatory cytokine induction. J Biol Chem 287:38665–38679

Cai M, Yu Z, Wang L, Song X, Zhang J, Zhang Z et al (2016) Tongxinluo reduces brain edema and inhibits post-ischemic inflammation after middle cerebral artery occlusion in rats. J Ethnopharmacol 181:136–145

Campos Y, Qiu X, Gomero E, Wakefield R, Horner L, Brutkowski W et al (2016) Alix-mediated assembly of the actomyosin-tight junction polarity complex preserves epithelial polarity and epithelial barrier. Nat Commun 7:11876

Choi C, Kwon J, Lim S, Helfman DM (2016) Integrin β1, myosin light chain kinase and myosin IIA are required for activation of PI3K-AKT signaling following MEK inhibition in metastatic triple negative breast cancer. Oncotarget 7:63466–63487

Clark K, Middelbeek J, Dorovkov MV, Figdor CG, Ryazanov AG, Lasonder E et al (2008) The alpha-kinases TRPM6 and TRPM7, but not eEF-2 kinase, phosphorylate the assembly domain of myosin IIA, IIB and IIC. FEBS Lett 582:2993–2997

Daquinag AC, Zhang Y, Amaya-Manzanares F, Simmons PJ, Kolonin MG (2011) An isoform of decorin is a resistin receptor on the surface of adipose progenitor cells. Cell Stem Cell 9:2011

Funami K, Matsumoto M, Obuse C, Seya T (2016) 14-3-3-zeta participates in TLR3-mediated TICAM-1 signal-platform formation. Mol Immunol 73:60–68

Garbuzova-Davis S, Mirtyl S, Sallot SA, Hernandez-Ontiveros DG, Haller E, Sanberg PR (2013) Blood-brain barrier impairment in MPS III patients. BMC Neurol 13:174

Greene C, Campbell M (2016) Tight junction modulation of the blood brain barrier: CNS delivery of small molecules. Tissue Barriers 4:e1138017

Ivanov AI, Bachar M, Babbin BA, Adelstein RS, Nusrat A, Parkos CA (2007) A unique role for nonmuscle myosin heavy chain IIA in regulation of epithelial apical junctions. PLoS ONE 2:e658

Kim T (2015) Determinants of contractile forces generated in disorganized actomyosin bundles. Biomech Model Mechanobiol 14:345–355

Kolega J (2006) The role of myosin II motor activity in distributing myosin asymmetrically and coupling protrusive activity to cell translocation. Mol Biol Cell 17:4435–4445

Kovács M, Tóth J, Hetényi C, Málnási-Csizmadia A, Sellers JR (2004) Mechanism of blebbistatin inhibition of myosin II. J Biol Chem 279:35557–35563

Liu W, Hendren J, Qin X, Shen J, Liu KJ (2009) Normobaric hyperoxia attenuates early blood-brain barrier disruption by inhibiting MMP-9-mediated occludin degradation in focal cerebral ischemia. J Neurochem 108:811–820

Liu WY, Wang ZB, Zhang LC, Wei X, Li L (2012) Tight junction in blood-brain barrier: an overview of structure, regulation, and regulator substances. CNS Neurosci Ther 18(8):609–615

Liu T, Ye Y, Zhang X, Zhu A, Yang Z, Fu Y et al (2016) Downregulation of non-muscle myosin IIA expression inhibits migration and

invasion of gastric cancer cells via the c-Jun N-terminal kinase signaling pathway. Mol Med Rep 13:1639–1644

Lu P, Chen J, Yan L, Yang L, Zhang L, Dai J, Hao Z, Bai T, Xi Y, Li Y, Kang Z, Xv J, Sun G, Yang T (2018) RasGRF2 promotes migration and invasion of colorectal cancer cells by modulating expression of MMP9 through Src/Akt/NF-κB pathway. Cancer Biol Ther 10:1–9

Luissint AC, Artus C, Glacial F, Ganeshamoorthy K, Couraud PO (2012) Tight junctions at the blood brain barrier: physiological architecture and disease-associated dysregulation. Fluids Barriers CNS 9:23

Lv Y, Fu L (2018) The potential mechanism for Hydroxysafflor yellow A attenuating blood-brain barrier dysfunction via tight junction signaling pathways excavated by an integrated serial affinity chromatography and shotgun proteomics analysis approach. Neurochem Int 112:38–48

Lv Y, Qian Y, Fu L, Chen X, Zhong H, Wei X (2015) Hydroxysafflor yellow A exerts neuroprotective effects in cerebral ischemia reperfusion-injured mice by suppressing the innate immune TLR4-inducing pathway. Eur J Pharmacol 769:324–332

Mashukova A, Wald FA, Salas PJ (2011) Tumor necrosis factor alpha and inflammation disrupt the polarity complex in intestinal epithelial cells by a posttranslational mechanism. Mol Cell Biol 31:756–765

Naydenov NG, Feygin A, Wang D, Kuemmerle JF, Harris G, Conti MA et al (2016) Nonmuscle Myosin IIA Regulates Intestinal Epithelial Barrier in vivo and Plays a Protective Role During Experimental Colitis. Sci Rep 6:24161

Neal CL, Xu J, Li P, Mori S, Yang J, Neal NN et al (2012) Overexpression of 14-3-3ζ in cancer cells activates PI3K via binding the p85 regulatory subunit. Oncogene 31:897–906

Nomura M, Shimizu S, Sugiyama T, Narita M, Ito T, Matsuda H et al (2003) 14-3-3 Interacts directly with and negatively regulates pro-apoptotic Bax. J Biol Chem 278:2058–2065

Pozuelo-Rubio M (2012) 14-3-3 Proteins are Regulators of Autophagy. Cells 1:754–773

Schuster TB, Costina V, Findeisen P, Neumaier M, Ahmad-Nejad P (2011) Identification and functional characterization of 14-3-3 in TLR2 signaling. J Proteome Res 10:4661–4670

Stamatovic SM, Johnson AM, Keep RF, Andjelkovic AV (2016) Junctional proteins of the blood-brain barrier: new insights into function and dysfunction. Tissue Barriers 4:e1154641

Turner JR (2006) Molecular basis of epithelial barrier regulation: from basic mechanisms to clinical application. Am J Pathol 169:1901–1909

Utech M, Ivanov AI, Samarin SN, Bruewer M, Turner JR, Mrsny RJ et al (2005) Mechanism of IFN-gamma-induced endocytosis of tight junction proteins: myosin II-dependent vacuolarization of the apical plasma membrane. Mol Biol Cell 16:5040–5052

Wang XT, Pei DS, Xu J, Guan QH, Sun YF, Liu XM et al (2007) Opposing effects of Bad phosphorylation at two distinct sites by Akt1 and JNK1/2 on ischemic brain injury. Cell Signal 19:1844–1856

Wang Y, Liu Q, Xu Y, Zhang Y, Lv Y, Tan Y et al (2016a) Ginsenoside Rg1 Protects against Oxidative Stress-induced Neuronal Apoptosis through Myosin IIA-actin Related Cytoskeletal Reorganization. Int J Biol Sci 12:1341–1356

Wang ZG, Cheng Y, Yu XC, Ye LB, Xia QH, Johnson NR et al (2016b) bFGF Protects Against Blood-Brain Barrier Damage Through Junction Protein Regulation via PI3K-Akt-Rac1 Pathway Following Traumatic Brain Injury. Mol Neurobiol 53:7298–7311

Wen H, Watry DD, Marcondes MC, Fox HS (2004) Selective decrease in paracellular conductance of tight junctions: role of the first extracellular domain of claudin-5. Mol Cell Biol 24:8408–8417

Wickman GR, Julian L, Mardilovich K, Schumacher S, Munro J, Rath N et al (2013) Blebs produced by actin-myosin contraction during apoptosis release damage-associated molecular pattern proteins before secondary necrosis occurs. Cell Death Differ 20:1293–1305

Wu JS, Cheung WM, Tsai YS, Chen YT, Fong WH, Tsai HD et al (2009) Ligand-activated peroxisome proliferator-activated receptor-gamma protects against ischemic cerebral infarction and neuronal apoptosis by 14-3-3 epsilon upregulation. Circulation 119:1124–1134

Zhai K, Tang Y, Zhang Y, Li F, Wang Y, Cao Z et al (2015) NMMHC IIA inhibition impedes tissue factor expression and venous thrombosis via Akt/GSK3β-NF-κB signalling pathways in the endothelium. Thromb Haemost 114:173

Zhaocheng J, Jinfeng L, Luchang Y, Yequan S, Feng L, Kai W (2016) Ginkgolide A inhibits lipopolysaccharide-induced inflammatory response in human coronary artery endothelial cells via down-regulation of TLR4-NF-κB signaling through PI3K/Akt pathway. Pharmazie 71(10):588–591

Zhou C, Wang Y, Peng J, Li C, Liu P, Shen X (2017) SNX10 Plays a Critical Role in MMP9 Secretion via JNK-p38-ERK Signaling Pathway. J Cell Biochem 118:4664–4671

Zhu Y, Bu Q, Liu X, Hu W, Wang Y (2014) Neuroprotective effect of TAT-14-3-3e fusion protein against cerebral ischemia/reperfusion injury in rats. PLoS ONE 9:e93334